

TRANSITION METALS IN LLANO VERMICULITE SAMPLES: AN EPR STUDY

P. M. SCHOSSELER¹ AND A. U. GEHRING^{2†}

¹ Laboratory for Physical Chemistry, Swiss Federal Institute of Technology, ETH,
CH-8092 Zürich, Switzerland

² Swiss Federal Institute for Forest, Snow and Landscape Research, WSL/ETH
CH-8903 Birmensdorf, Switzerland

Abstract—Continuous wave and pulsed electron paramagnetic resonance spectroscopies combined with thermal and chemical methods were used to identify and characterize V(IV), Fe(III), Mn(II) and Cr(III) in a multimineral system that consists of vermiculite and impurities of carbonates. All of these transition metals were structure-bound in mineral phases. The V(IV) was located in octahedral layers of the vermiculite and became oxidized to V(V) during the transformation of the host mineral to enstatite at about 800 °C. The Fe(III) was associated with the vermiculite as well as the carbonate impurities. The Fe(III) identified in the vermiculite was transferred into the enstatite structure during the thermal conversion. An indirect proof of Fe(III) and Cr(III) in the impurities was found in the heated samples in which these cations occurred in Ca and/or Mg oxides that were formed by transformation of the carbonates. The Mn(II) in the untreated samples was associated with the impurities and was also detected in oxides formed from the samples heated at 600 °C.

Key Words—Carbonates, Cw and Pulsed Electron Paramagnetic Resonance Spectroscopies, Phase Transformation, Vermiculite.

INTRODUCTION

Electron paramagnetic resonance (EPR) spectroscopy is an analytical tool often used for the identification and characterization of paramagnetic transition metals associated with minerals (Calas 1988). Continuous-wave (cw) spectra obtained from monomineral systems permit the description of the chemical environment and binding properties of paramagnetic species such as Fe(III), Mn(II) and V(IV) (McBride 1990). The assignment of an EPR signal recorded from a multimineral natural system, such as a soil, to a specific mineral phase or a specific chemical form is often difficult because of spectral superposition of paramagnetic species (Gehring et al. 1994). An experimental approach based on the changes in EPR signals upon thermal or chemical treatment was developed to accurately characterize the chemical environment of paramagnetic cations within multimineral systems (Angel and Vincent 1978; Gehring and Karthein 1990; Gehring et al. 1993a). This approach is based on the assumption that different chemical forms or different mineral phases of a multimineral system differ in thermal and/or chemical stability. Ambiguities can arise if paramagnetic cations are located in traces of mineral phases which can neither selectively be dissolved nor be distinguished by their thermal behavior (McBride 1995; Gehring and Sposito 1995). In addition, one has to be aware that paramagnetic cations in different mineral phases can have sim-

ilar ligand fields. This can result in spectra with EPR parameters, for example, hyperfine splitting constants and g-values, which are not significantly different. The application of pulsed EPR techniques provides a possibility to overcome such difficulties for the assignment of paramagnetic species. Electron spin echo envelope modulation (ESEEM) is a technique that can give information on the nuclear spin environment of paramagnetic centers if the hyperfine coupling between electrons and the surrounding nuclei are too small to be resolved in cw EPR (Schweiger 1991). Weakly coupled nuclei give characteristic peaks in ESEEM, which permit the calculation of the nuclear g-factor (g_N). One peak occurs at the nuclear Zeeman frequency (ν) and the other is considered a sum peak at twice this frequency (2ν). Strongly coupled nuclei within disordered systems such as powder samples yield broad spectral features if the coupling is sufficiently anisotropic. The time signal of these features often decays in the spectrometer dead time and only the narrow sum peak is detectable. A detailed description of the method can be found elsewhere (Mims 1972; Kevan 1979; Dikanov and Astahikin 1989).

Pulsed EPR techniques have been widely used in chemistry and biochemistry whereas natural multimineral systems have not been studied (Mims and Peisach 1981; Möhl et al. 1990; Karthein et al. 1991). The purpose of this research was to apply cw and pulsed EPR in combination with chemical and thermal treatment to identify and characterize paramagnetic species in vermiculite-rich samples from Llano, Texas.

† Present address: Institute of Terrestrial Ecology ETH Zurich Grabenstrasse 3 CH 8952 Schlieren Switzerland.

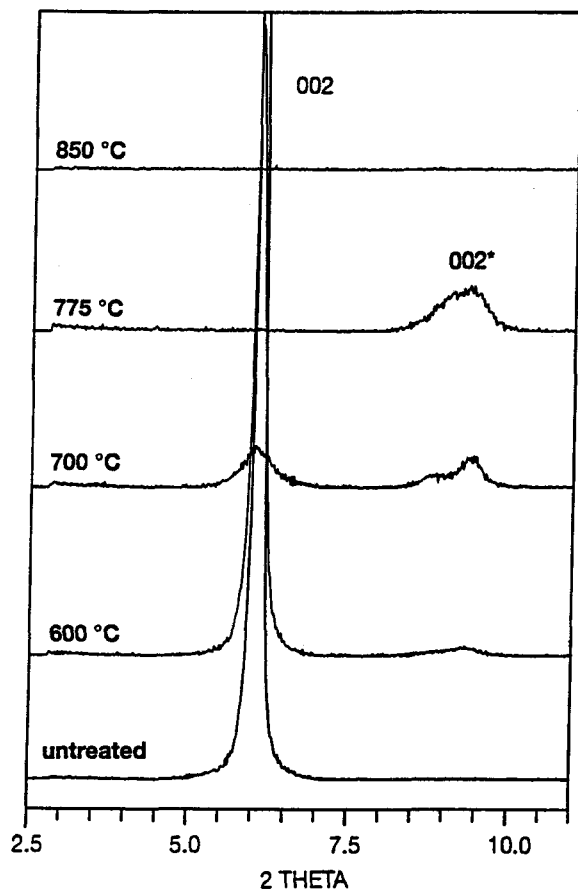


Figure 1. Powder XRD of an untreated vermiculite sample and after stepwise heating at different temperatures.

SAMPLES AND METHODS

The Llano vermiculite from Texas is a weathering product of phlogopite contained in a dolomitic and magnesian marble (Clabaugh and Barnes 1959). The vermiculite (VTX-1) was obtained from the Clay Minerals Society's Source Clay Repository. Different sets of handpicked vermiculite flakes were ground in a ball mill with a teflon vessel and an agate ball clamped within a dismembrator. Untreated and heated powder samples were analyzed by X-ray diffractometry (XRD, SCINTAG XDS 2000) using $\text{CuK}\alpha$ radiation. Spectroscopic analyses were performed on untreated samples and samples that were heated progressively in an oven from 500 to 1100 °C for 12 h at each step, then cooled and stored under air contact. Fourier-transform infrared (FTIR) spectra in the wavenumber range 400–4000 cm^{-1} were recorded on a Nicolet 510P spectrometer. The FTIR spectra were obtained in transmittance mode on pellets containing 1.5 mg sample in 300 mg KBr.

The cw EPR spectra were recorded at room temperature (RT) on a Bruker ESP 300 spectrometer. The

spectra were measured at a microwave frequency of 9.44 GHz with a micropower of 5 mW, a modulation amplitude of 0.5 mT and a modulation frequency of 100 kHz. The g -values and the line widths were determined with a Bruker NMR Gaussmeter ER 035M and a HP 5248M Electronic Frequency Counter using *N,N*-diphenylpicrylhydrazyl (DPPH) as a control marker. The spin concentration of the Cr(III) species was estimated by double integration of the EPR signals after subtraction of the base line. The cw EPR analysis was also performed on samples after chemical treatment. To dissolve the impurities, the sample was treated with 0.37 M HCl at 83 °C for 2 h (Suquet et al. 1991). To study the exchangeability of paramagnetic cations, 0.5 g samples were equilibrated at pH 4.5 with 20 g of a solution containing 0.01 mol kg^{-1} EDTA and 1 mol kg^{-1} KNO_3 . The suspensions were stirred for 16 h at RT, then filtered and washed with deionized water and air-dried. In addition, the samples were treated with 30% H_2O_2 to determine the resistance of the paramagnetic cations against oxidation.

Two-pulse electron spin echo envelope modulation (ESEEM) measurements at 3.7 K were performed on untreated samples and samples heated to 700 and 900 °C. To exclude that paramagnetic species such as V(III) and Fe(II), which give no EPR signal at RT, contributed to the pulse EPR measurements at 3.7 K, echo-detected EPR experiments were carried out (Schweiger 1991). For the ESEEM measurements, a home-built spectrometer equipped with an Oxford CF935 cryostat was used (Fauth et al. 1986). Two-pulse echo sequences with pulse length of 20/40 and 100/200 nsec were applied. The time increment between the two pulses was 10 ns, the repetition rates were 0.1 kHz for the untreated sample and 1 kHz for the other ones. The time signals were converted to frequency spectra by Fourier transformation after subtraction of the unmodulated part of the echo envelope, apodization with a sine-bell function and/or Hamming window function, as well as zero-filling to 1024 points. Magnitude spectra were calculated because of the spectrometer dead time.

RESULTS

Vermiculite was the only mineral found by XRD in the untreated sample. Upon heating to 850 °C the diffraction lines of vermiculite vanished. At this temperature, a diffraction pattern characteristic of enstatite (JCPDS, 1980) appeared that did not change upon further heating to 1100 °C. Simultaneously, several minor peaks, which could not be assigned to a specific mineral phase, occurred. A d -spacing of 1.448 nm was found for the untreated vermiculite as indicated by the (002) diffraction line (Figure 1). Upon heating to 600 °C a new peak appeared around 0.95 nm considered as (002)*. Further heating to 700 °C led to a decrease of the (002) diffraction line and an increase of the

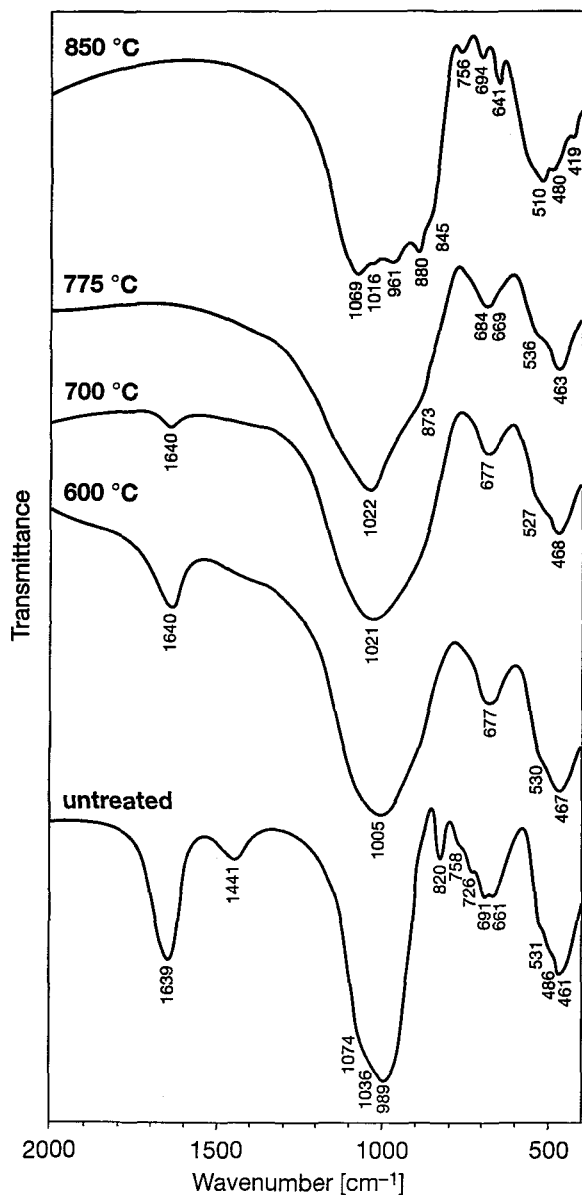


Figure 2. FTIR spectra of an untreated vermiculite sample and after stepwise heating at different temperatures.

(002)* reflection. Heating to 775 °C lead to the disappearance of the (002) reflection and at 850 °C, the (002)* peak vanished as well (Figure 1). The decomposition of the vermiculite was also observed by FTIR. In the range from 2000 to 1200 cm^{-1} , the spectrum of the untreated sample showed two bands at 1639 and at 1441 cm^{-1} (Figure 2). The band at 1639 cm^{-1} can be attributed to molecular vibration of water. The 1441 cm^{-1} band is typical of the asymmetric stretch vibration of CO_3^{2-} for carbonates such as magnesite (MgCO_3) or dolomite ($\text{CaMg}(\text{CO}_3)_2$), impurities known to occur with the Llano vermiculite (Jones and

Jackson 1992; Suquet et al. 1991). In the mid-infrared region, all bands characteristic of the Llano vermiculite sample (Suquet et al. 1991; Farmer 1974) were found: Si-O stretching bands (989 and 461 cm^{-1}), mixed Si-O/Al-O vibrations (820 cm^{-1}), several bands and shoulders attributed to mixed Si-O/Al-O/Al-O-Si vibrations (758, 726, 691 and 661 cm^{-1}) and two shoulders that can be attributed to Mg-O stretching (531 and 486 cm^{-1}). Upon heating to 600 °C, the band at 1441 cm^{-1} disappeared and the Si-O stretching bands around 1000 and 460 cm^{-1} broadened (Figure 2). The shoulders at 758 and 726 cm^{-1} vanished and only a single band at 677 cm^{-1} was observed (Figure 2). For treatment at 700 °C, the Si-O stretching band around 1000 cm^{-1} showed further broadening. Heating to 775 °C led to the disappearance of the band at 1639 cm^{-1} , a marked shoulder at 873 cm^{-1} was generated, and the Mg-O stretching band (536 cm^{-1}) became more pronounced. A drastic change in the mid-infrared range was observed upon heating to 850 °C. The broad feature around 1000 cm^{-1} became structured with bands at 1069, 1016, 961 and 880 cm^{-1} and a shoulder at 845 cm^{-1} . Again, bands around 760 and 690 cm^{-1} were found. A new band appeared at 641 cm^{-1} and the band around 460 cm^{-1} became structured with peaks at 510, 480 and 419 cm^{-1} . The newly formed FTIR pattern upon heating to 850 °C was characteristic of enstatite (Bilton et al. 1972). No significant spectral changes were observed upon further heating to 1100 °C.

The EPR spectrum of the untreated sample exhibited two groups of resonances around $g = 4.3$ and $g = 2$ (Figure 3). The low-field resonance at $g = 4.3$ is characteristic of Fe(III) located in sites with rhombic symmetry. The shoulders around 4.3 indicated that part of the Fe(III) sites did not have maximum rhombic character (Meads and Malden 1975). The spectrum around $g = 2$ showed a superposition of an eight-line and a six-line hyperfine-split (HFS) signal (Figure 3), that can be attributed to V(IV) and Mn(II), respectively. The intensity of the six-line HFS of Mn(II) varied within the samples obtained from the different sets of handpicked platelets (Figure 3).

The Fe(III), Mn(II) and V(IV) signals were resistant against chemical treatments with 30% H_2O_2 and EDTA. After the treatment with 0.37M HCl the signals at $g \approx 2$ had disappeared and the Fe(III) signal changed into a single asymmetric line with $g = 4.27$ (Figure 4). Simultaneously a broad signal centered at $g \approx 2$ with a line width of 34 ± 1 mT occurred, which is typical for iron oxides such as hematite or magnetite (Gehring and Karthein 1990).

Upon heating, the Fe(III) signal, which was stable up to 1000 °C, became more isotropic and the g -value shifted slightly to 4.27 ± 0.01 (Figure 5). The Mn(II) and V(IV) spectra behaved differently with thermal treatment. Above 500 °C two new sharp signals ap-

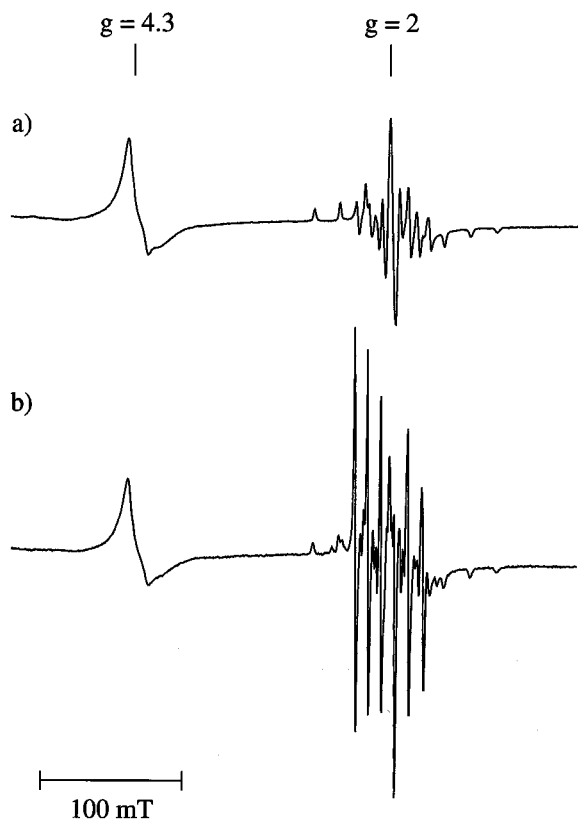


Figure 3. Wide-range EPR spectra of untreated samples poor (a) and rich (b) in Mn(II) recorded at RT.

peared and at 1000 °C a broad signal was formed at $g \approx 2$ (Figure 5).

The eight-line V(IV) spectra arising from the interaction of the electron spin with the nuclear spin ($I = 7/2$) of ^{51}V (99.8% natural abundance), showed g and A tensors with parallel and perpendicular components (Figure 6). For the parallel component, $g_{\parallel} = 1.941 \pm 0.001$, $A_{\parallel} = 18.11 \pm 0.07$ mT, and for the perpendicular component $g_{\perp} = 1.985 \pm 0.001$, $A_{\perp} = 7.05 \pm 0.02$ mT were obtained. These EPR parameters were similar to those reported for the Llano vermiculite by McBride (1990). The V(IV) signal was stable up to 500 °C. Further heating led to a decrease in intensity and at 800 °C the signal had vanished. Simultaneously to the most pronounced decrease in intensity of the V(IV) spectrum between 600 and 700 °C, a sharp signal with $g = 2.002 \pm 0.001$ and a line width of 0.36 ± 0.01 mT appeared (Figure 6). Computer simulated subtraction of the remaining V(IV) signal revealed the symmetric shape of the newly formed one. This signal became weaker upon heating to 800 °C and disappeared at 850 °C.

The Mn(II) spectra of the untreated samples consisted of six dominant lines separated by five weaker doublets. The six lines correspond to the central trans-

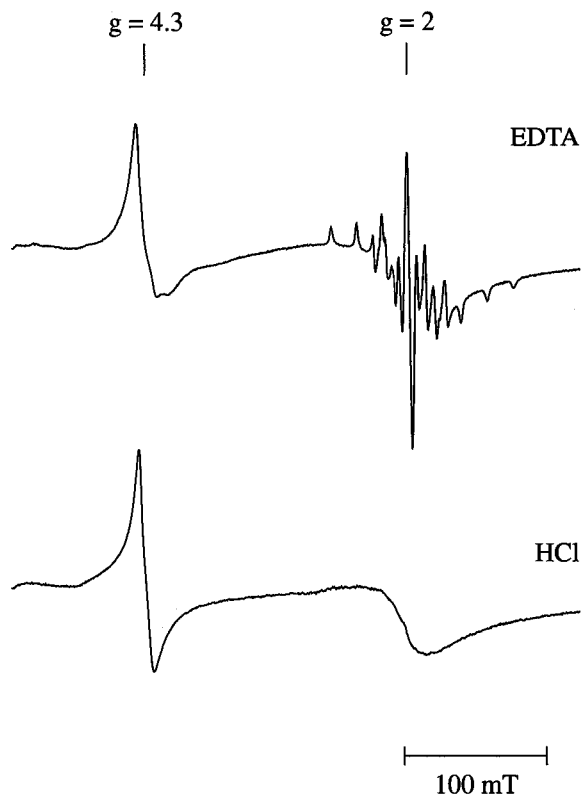


Figure 4. Wide-range EPR spectra of Mn(II)-poor sample after chemical treatment with EDTA and HCl.

sition between the electronic states $M_s = \pm 1/2$, which is split by the hyperfine interaction with the nuclear spin ($I = 5/2$) of ^{55}Mn (100% natural abundance). The five doublets correspond to forbidden transitions, $\Delta M_s = \pm 1$ ($\Delta m_l = \pm 1$), and are caused by axial distortion of the crystal field (Mankowitz and Low 1970). The Mn(II) signals of the untreated samples were characterized by $g = 2.002 \pm 0.002$ and HFS of $A = 9.44 \pm 0.03$ mT (Figure 7). Upon heating to 500 °C the signal intensity decreased but no significant changes of the spectral parameters occurred. The line width of the six HF components became more narrow and more structure was discernible. Upon heating to 600 °C, it led to both a drastic decrease in signal intensity and a spectral change. The new six-line HFS signal with $g = 2.002 \pm 0.001$ and $A = 8.70 \pm 0.02$ mT regained intensity upon heating to 800 °C and was stable at 1000 °C (Figure 7). At temperatures above 800 °C, the shape of the Mn(II) spectra indicated an overlay by two other EPR signals. These signals were found before for heated vermiculite samples from Llano but they were not assigned in detail (Gehring et al. 1994). One signal with $g = 2.004 \pm 0.001$ occurred between the third and the fourth HF component of the Mn(II) signal and was attributed to Fe(III) in cubic symmetry (Beltrán-López and Castro-Tello 1980). The other sig-

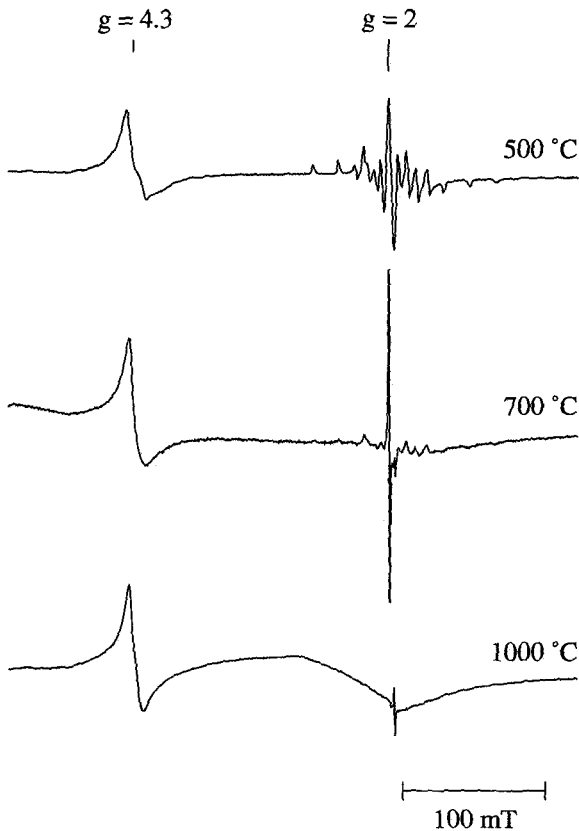


Figure 5. Wide-range EPR spectra of Mn(II)-poor sample recorded at RT after stepwise heating to 500, 700 and 1000 °C.

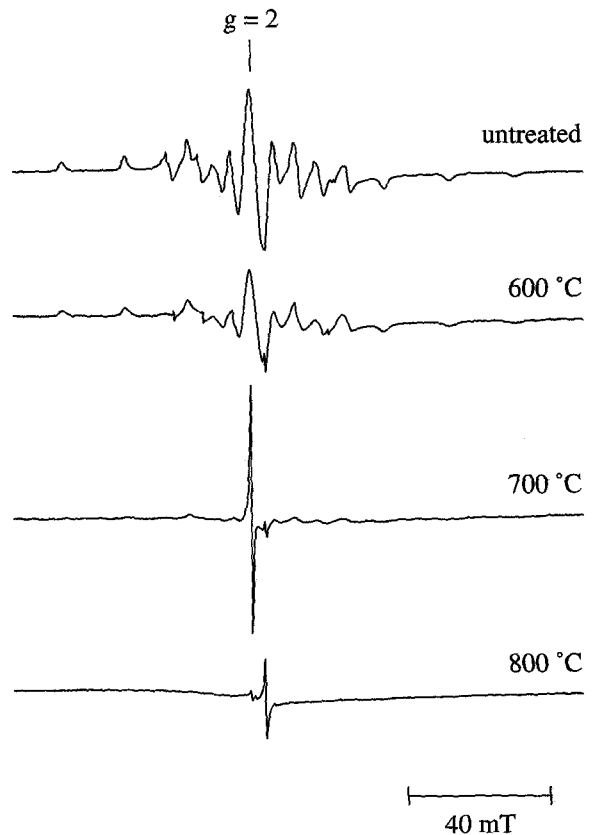


Figure 6. Narrow-range EPR spectra at RT of an untreated Mn(II)-poor sample and after stepwise heating to 600, 700 and 800 °C.

nal with $g < 2$ was indicated by an enhanced intensity of the fourth HF component of the Mn(II) spectra (Figure 7). The $g < 2$ signal was clearly detected in the Mn-poor sample heated at 600 °C (Figure 6). At higher temperatures, the signal intensity increased and a maximum was reached at 900 °C. The signal exhibited an intense central line with $g = 1.979 \pm 0.001$ and four HF components with $A = 1.79 \pm 0.01$ mT (Figure 8). Such a signal was described for Cr(III) in solids with cubic symmetry (Low 1957a). The sharp central line with a width of 0.15 ± 0.01 mT arose from Cr isotopes (^{50}Cr and ^{52}Cr) without nuclear spin. The four weak components were characteristic of HFS of ^{53}Cr isotopes ($I = 3/2$ natural abundance 9.5%). Double integration over the central line and the satellite lines and the comparison of the signal intensities gave an experimental value of $9 \pm 2\%$ for the ^{53}Cr isotopic abundance.

The echo-detected EPR experiments revealed the same paramagnetic species in the $g = 2$ region at 3.7 K as at RT. All ESEEM decayed within 1 and 2 μs at 3.7 K (Figure 9a and 9c). The short phase memory times can be caused by the interaction with other paramagnetic species such as Fe(III). The ESEEM with

20 and 40 ns pulses obtained from the central V(IV) feature near $g = 2$ position of the untreated sample showed only little modulation (Figure 9a). The magnitude spectrum after Fourier transformation consisted of a broad peak at 3.4 ± 0.5 MHz with a shoulder at about 6.5 MHz, and a weaker peak at 13.9 ± 0.5 MHz. The peaks indicated two different nuclear Zeeman frequencies (ν). The experimental accuracy was strongly influenced by the rapid decay of ESEEM that resulted in a broad spectral line (Figure 9b). The weak line leading to a nuclear g factor ($|g_N|$) of 5.46 ± 0.2 was characteristic of protons ($|g_N| = 5.5854$ natural abundance 99.985%). The maximum of the intense line corresponded to a $|g_N|$ value of 1.35 ± 0.2 , and the shoulder with approximately twice this value coincided with the sum peak. These values were close to those for weakly coupled nuclei of diamagnetic ^{27}Al ($I = 5/2$ 100% natural abundance $|g_N| = 1.4554$). Other elements with similar $|g_N|$ values were ruled out because of their paramagnetic nature or their absence within the vermiculite specimen. For the sample heated to 700 °C the ESEEM spectrum obtained from the $g = 2$ position, where the new sharp signal overlapped the remaining V(IV) one, a peak corresponding to $|g_N| =$

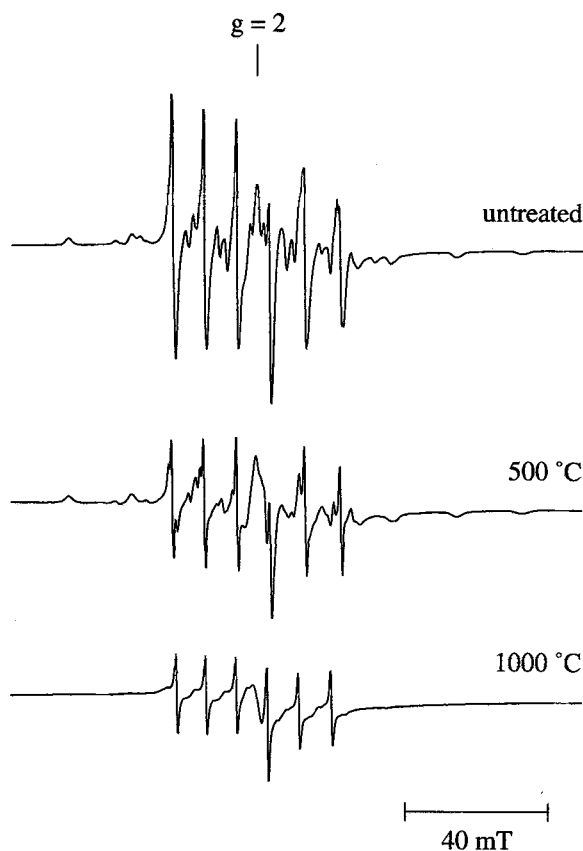


Figure 7. Narrow-range EPR spectra at RT of an untreated Mn(II)-rich sample and after stepwise heating to 500 and 1000 °C.

1.34 ± 0.2 was found (data not shown). However, an accurate assignment of the ESEEM spectrum was not possible because of the overlap of the EPR signals at $g = 2$. The ESEEM at the position $g = 1.98$ assigned to Cr(III) of the sample heated at 900 °C led to a magnitude ESEEM spectrum with a single line at 0.9 ± 0.2 MHz corresponding to $|g_N| = 0.35 \pm 0.08$ (Figure 9d). This value was close to $|g_N| = -0.3419$ for diamagnetic ^{25}Mg ($I = 5/2$ natural abundance 10.13%).

DISCUSSION

The vermiculite flakes contain differing amounts of carbonate impurities, dolomite or magnesite, as indicated by FTIR spectroscopy. Although the concentration of these impurities is too low to be detected by XRD, for the investigation by EPR spectroscopy, the sample has to be considered a multimineral system. Since vermiculite is attacked by acids (Suquet et al. 1991), the carbonates are not removed by selective dissolution. Thus, the paramagnetic transition elements detected by EPR spectroscopy (Figure 3) can be attributed to the vermiculite and/or the carbonate im-

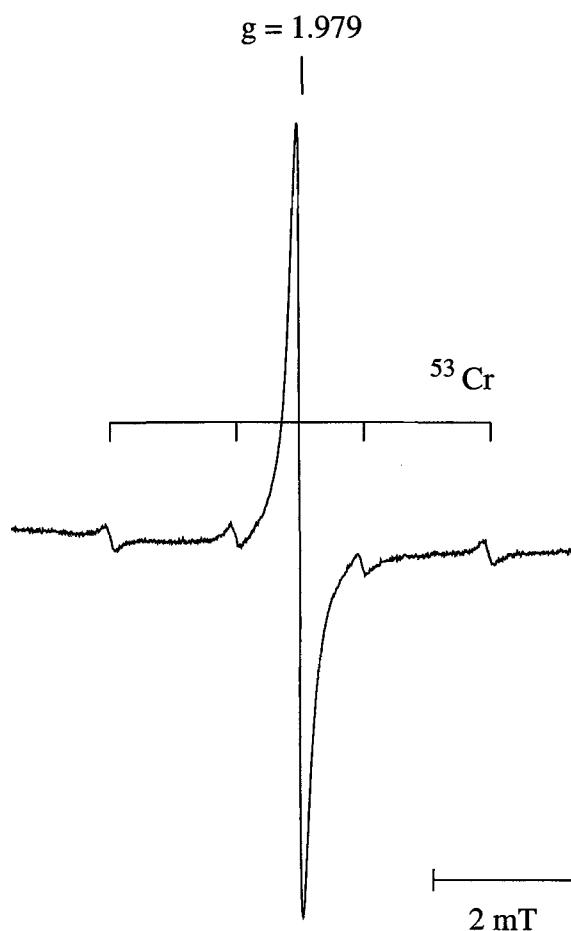


Figure 8. Narrow-range EPR spectra of Cr(III) signal generated upon heating to 900 °C. The HFS of the ^{53}Cr signal is indicated. The EPR parameters were modulation amplitude 0.01 mT and 10 scans.

purities. The well resolved EPR signals and their resistance against EDTA and H_2O_2 show that these cations cannot form clusters or occur as adsorbates, and must therefore be structure-bound in mineral phases (Gehring et al. 1993b).

The EPR signal at $g = 4.3$ can be attributed to isolated Fe(III) structure-bound in the vermiculite since such a signal has often been found for other phyllosilicates (Meads and Malden 1975; Olivier et al. 1975). This assignment agrees well with the spectral change upon heating and after acid treatment, which can be explained by an increase in the rhombic character of the Fe(III) ligand field (Meads and Malden 1975).

The comparison of the EPR spectra at $g = 2$ of the different sample sets reveals that in contrast to the Mn(II), the V(IV) concentration does not change significantly (Figure 3). McBride (1990) suggested that V(IV) is structure-bound in the vermiculite. This assignment is supported by the disappearance of the signal upon heating to 800 °C, the temperature at which

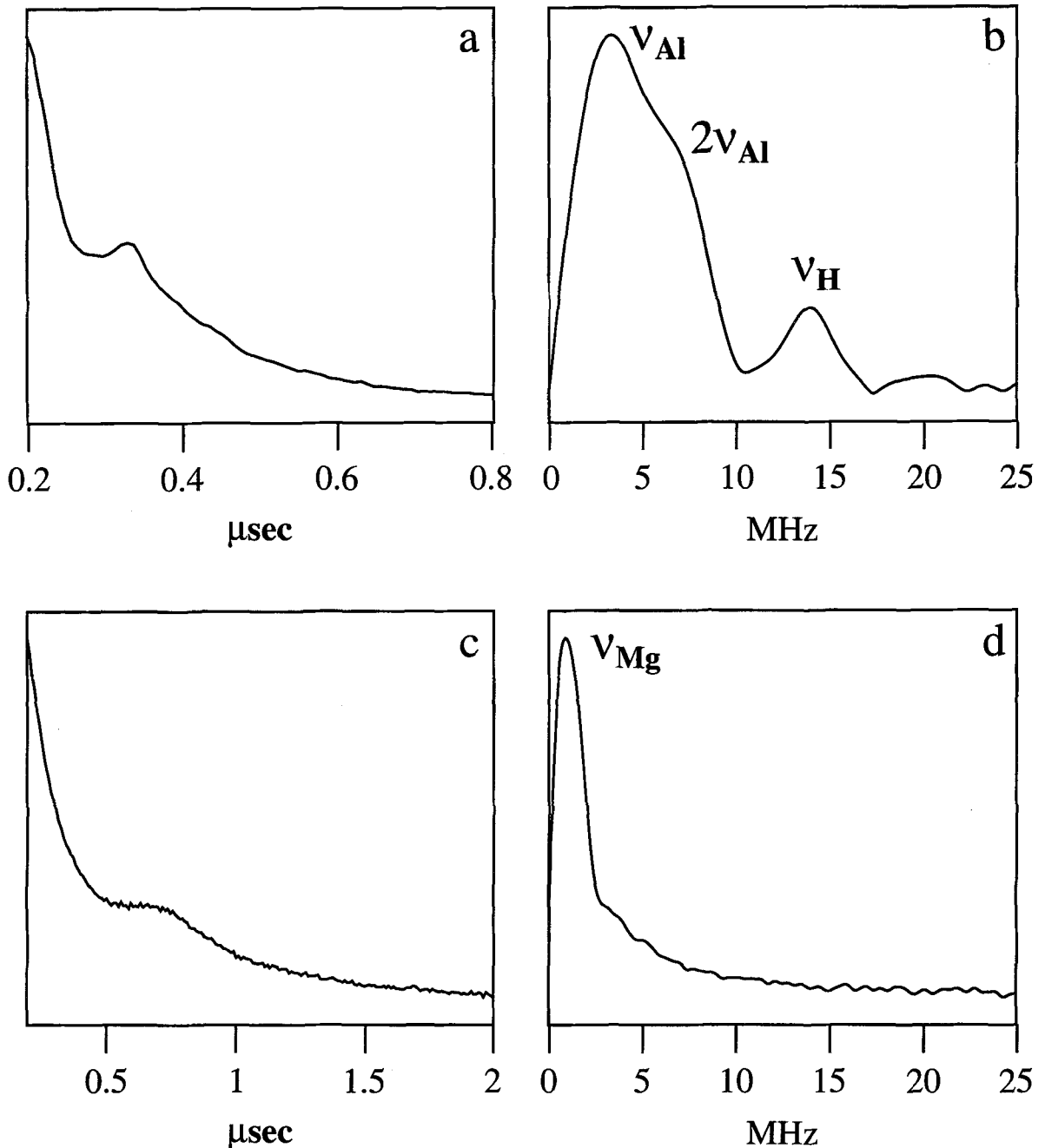


Figure 9. Two-pulse ESEEM pattern of the untreated Mn(II)-poor sample recorded at the $g = 2$ position (a), of the sample heated at $900\text{ }^{\circ}\text{C}$ recorded at the $g = 1.979$ position (c) and corresponding Fourier transformed ESEEM magnitude spectra (b) and (d). The nuclear Zeeman frequencies ν_{Al} and ν_{H} , as well as the sum peak $2\nu_{\text{Al}}$ (b) and the nuclear Zeeman frequency ν_{Mg} (d) are indicated.

vermiculite converts to enstatite as indicated by XRD and FTIR (Figures 1 and 2). The disappearance of the signal can be explained by oxidation of V(IV) to diamagnetic V(V) during the break-down of the host mineral. In the vermiculite, V(IV) could be located in octahedral or tetrahedral sites.

The presence of Al in its vicinity found by ESEEM measurements gives no clues to the exact location of V(IV) since Al can occupy both sites in the vermiculite (Herrero et al. 1985). By contrast, the presence of protons near V(IV) argues in favor of a coordination in octahedral layers that contain hydroxyl groups. Fur-

ther evidence derives from the disappearance of the V(IV) signal for the HCl-exposed samples, since such a treatment preferentially dissolves the octahedral layers (Suquet et al. 1991). Finally, the assignment to octahedral sites agrees with the known coordination chemistry of V(IV) with oxygen ligands, which shows that V(IV) in tetrahedra is very unlikely (Butler 1990).

For the temperature range in which vermiculite destabilizes (Figures 1 and 2), a sharp signal with no HFS dominates the spectrum at $g = 2$ (Figure 6). The shape of this signal and the closeness of its g -value to that of a free electron strongly suggests that this newly formed signal is the result of a structural defect. Since the signal disappears at 850 °C, the temperature at which the transformation of vermiculite to enstatite is completed, it is unlikely that the defect structure is associated with the carbonate impurities. However, defects associated with phyllosilicates have often been observed but they are generally unstable upon heating to 400 °C (Jones et al. 1974; Gehring et al. 1993b). A possible explanation of the uncommon thermal stability is the formation of a metastable, disordered phase. Vermiculite converts to enstatite via a non-swelling phase described as biopyribole (Suquet et al. 1984). The generation of such a polysome starts at about 600 °C and is completed at 775 °C as indicated by the XRD peak at 0.95nm (Figure 1). Structural disorder based on defects in the slip sequence of biopyribole has been demonstrated by transition electron microscopy (Veblen and Buseck 1980; Veblen 1991). Considering the structure model by Suquet et al. (1984) and the thermal stability of the sharp signal, it can be argued that the structural defect is the result of an epitaxial growth of enstatite along the (010) plane of vermiculite during the generation of the biopyribole.

The Mn(II) is inhomogeneously distributed throughout the samples and shows a different thermal behavior than V(IV). Therefore, it is likely that Mn(II) is not structure-bound in the vermiculite. The shape of the six-line feature at 500 °C is similar to that of Mn(II) replacing Mg and Ca in two sites of dolomite (Lloyd et al. 1993; Wildemann 1970). This carbonate is a major compound of the marble that contains the vermiculite (Clabaugh and Barnes 1959). Thus, it can be postulated that part of the Mn(II) is in dolomite impurities. Since the spectral parameters of Mn(II) of the untreated sample and after heating to 500 °C are similar but the signal shapes are different, it is very likely that Mn(II) is associated with chemically varying Mg-rich members of the CaCO_3 - MgCO_3 solid solution series (Wildemann 1970). The decrease in signal intensity upon heating suggests that Mn(II) in the carbonates is protected differently from oxidation. Following these argumentations, the spectral changes above 600 °C of the remaining Mn(II) can be explained by the conversion of the carbonates into oxides. The parameters of the newly formed six-line sig-

nals are characteristic of Mn(II) in both Ca and Mg oxides (Low 1957b; Wildemann 1970).

The Cr(III) and Mn(II) spectra show a similar thermal behavior. At higher temperatures, both cations are coordinated in mineral phases with cubic symmetry. Therefore, it can be postulated that Cr(III) at these temperatures is also structure-bound in Ca and Mg oxides. The assignment to the latter is supported by ESEEM spectra that reveal Mg in the vicinity of Cr(III). Thus, it is very likely that this cation is also present in the carbonate impurities of the untreated sample. The low concentration, as well as the broad EPR signal for Cr(III) in non-cubic solids, can explain the lack of direct evidence for Cr(III) in the carbonate impurities. Following this argumentation, it cannot be excluded that part of Cr(III) is associated with the vermiculite and at higher temperatures with enstatite.

In analogy to Cr(III), the occurrence of an Fe(III) signal at $g = 2$ in the samples heated above 600 °C indicates that Fe(III) is located within earth alkaline oxides and therefore also in the carbonate precursors. In contrast to Cr(III), Fe(III) is also unambiguously found in the vermiculite. Furthermore, the generation of a broad signal with $g \approx 2$ at 1000 °C suggests that part of the Fe(III) is released from silicate or Mg and Ca oxides to form a ferric oxide, most likely hematite (Gehring and Karthein 1990).

CONCLUSIONS

The experimental approach combining cw and pulsed EPR spectroscopies with chemical and thermal treatment was applied to identify and characterize the transition elements Fe(III), Mn(II), V(IV) and Cr(III) for multiminerall samples that contain vermiculite and impurities of carbonates. The analysis of the data led to the following assignments:

- 1) The V(IV) occurs as an isomorphically substituted species in the octahedral sheets of the vermiculite. During the thermal break down of the vermiculite, V(IV) is metastable and becomes completely oxidized.
- 2) The Fe(III) detected in the untreated sample is located in the vermiculite and is incorporated into the enstatite structure upon heating.
- 3) The Mn(II) is mainly associated with the carbonates and part of it survives the thermal conversion of the host minerals into Ca and/or Mg oxides.
- 4) The presence of Cr(III) and Fe(III) in the impurities are indirectly proven by the detection of these paramagnetic species in the oxides with cubic symmetries formed during thermal transformation of the carbonates.
- 5) During the transformation of the vermiculite to enstatite via a biopyribole, defect structures are generated in the metastable polysome.

ACKNOWLEDGMENTS

The authors are grateful to S. Zimmermann for providing the XRD measurements and to J. Luster for the FTIR analysis. The authors appreciate A. Schweiger and J. Luster for their valuable comments on the manuscript, and to P. Hall for his critical review.

REFERENCES

- Angel BR, Vincent WEJ. 1978. Electron spin resonance studies of iron oxides associated with the surface of kaolins. *Clays & Clay Miner* 26:263–272.
- Beltrán-López V, Castro-Tello J. 1980. ESR lineshapes in polycrystalline samples: $^{6}\text{S}_{5/2}$ ions in axial and cubic crystal fields. *J Magn Reson* 39:437–460.
- Bilton MS, Gilson TR, Webster M. 1972. The vibration spectra of some chain type silicate minerals. *Spectrochim Acta* 28A:2113–2119.
- Butler A. 1990. The coordination and redox chemistry of vanadium in aqueous solutions. In: Chasteen NE, editor. Vanadium in biological systems. Dordrecht: Kluwer Academic Publ. p 25–49.
- Calas G. 1988. Electron paramagnetic resonance. In: Hawthorn FC, editor. Spectroscopic methods in mineralogy and geology. *Rev Miner* 18:513–571.
- Clabaugh SE, Barnes VE. 1959. Vermiculite in central Texas. *Texas Univ Bur Econ Geol Rept Invest* p 40–45.
- Dikanov SA, Astahikin AV. 1989. ESEEM of disordered systems: Theory and applications. In: Hoff AJ, editor. Advanced EPR, applications in biology and biochemistry. Amsterdam: Elsevier. p 59–115.
- Farmer VC. 1974. The infrared spectra of minerals. London: Mineralogical Society. 539 p.
- Fauth J-M, Schweiger A, Braunschweiler L, Forrer J, Ernst RR. 1986. Elimination of unwanted echoes and reduction of dead time in three-pulse electron spin-echo spectroscopy. *J Magn Reson* 66:74–85.
- Gehring AU, Karthein R. 1990. An ESR and calorimetric study of iron oolitic samples from the Northampton ironstone. *Clay Miner* 25:303–311.
- Gehring AU, Fry IV, Luster J, Sposito G. 1993a. Vanadium (IV) in a multimineral lateritic saprolite: A thermoanalytical and spectroscopic study. *Soil Sci Soc Am J* 57:868–873.
- Gehring AU, Fry IV, Luster J, Sposito G. 1993b. The chemical form of vanadium(IV) in kaolinite. *Clays & Clay Miner* 41:662–667.
- Gehring AU, Schosseler PM, Luster J. 1994. The chemical form of Mn(II) and V(IV) in mineral phases as determined by EPR spectroscopy. *Miner Mag* 58A:323–324.
- Gehring AU, Sposito G. 1995. Residual manganese(II) speciation in montmorillonite: A reply. *Clays & Clay Miner* 43:385–386.
- Herrero CP, Sanz J, Serratos JM. 1985. Si and Al distribution in micas: Analysis by high-resolution Si NMR spectroscopy. *J Phys C, Solid State Phys* 18:13–22.
- Joint Committee on Powder Diffraction Standards (JCPDS). 1980. Mineral powder diffraction file, data book. Swarthmore, PN:JCPDS international center for diffraction data.
- Jones GC, Jackson B. 1992. Infrared transmission spectra of carbonate minerals. London: Chapman & Hall.
- Jones JPE, Angel BR, Hall PL. 1974. Electron spin resonance of synthetic kaolinite II. *Clay Miner* 10:257–270.
- Karthein R, Motschi H, Schweiger A, Ibric S, Sulzberger B, Stumm W. 1991. Interaction of chromium(III) complexes with hydrous $\delta\text{-Al}_2\text{O}_3$: Rearrangements in the coordination sphere studied by electron spin resonance and electron spin-echo spectroscopies. *Inorg Chem* 30:1606–1611.
- Kevan L. 1979. Modulation of electron spin-echo decay in solids. In: Kevan L, Schwartz RN, editors. Time domain electron spin resonance. New York: Wiley. p 279–341.
- Lloyd RV, Morrison JW, Lumsden DN. 1993. The influence of ferrous and ferric iron on the Mn^{2+} partitioning ratio and ESR signal of synthetic dolomite. *Geochim Cosmochim Acta* 57:1071–1078.
- Low W. 1957a. Paramagnetic resonance and optical absorption spectra of Cr^{3+} in MgO. *Phys Rev* 105:801–805.
- Low W. 1957b. Paramagnetic resonance of manganese in cubic MgO and CaF_2 . *Phys Rev* 105:793–800.
- Mankowitz J, Low W. 1970. Forbidden transitions ($\Delta m = \pm 1$) in the paramagnetic resonance absorption of Mn^{2+} in calcite. *Phys Rev B* 2:28–32.
- McBride MB. 1990. Electron spin resonance spectroscopy. In: Perry DL, editor. Instrumental surface analysis of geological materials. New York: VCH Publ. p 233–281.
- McBride MB. 1995. Comment on the natural Mn(II) EPR signal of SWy-1 montmorillonite. *Clays & Clay Miner* 43:383–384.
- Meads RE, Malden PJ. 1975. Electron spin resonance in natural kaolinites containing Fe^{3+} and other transition metal ions. *Clay Miner* 10:313–345.
- Mims WB. 1972. Envelope modulation in spin-echo experiments. *Phys Rev B* 5:2409–2419.
- Mims WB, Peisach J. 1981. Electron spin echo spectroscopy and the study of metalloproteins. In: Berliner LJ, Reuben J, editors. Biological magnetic resonance, vol. 3. New York: Plenum. p 213–263.
- Möhl W, Schweiger A, Motschi H. 1990. Modes of phosphate binding to copper(II): Investigation of the electron spin echo envelope modulation of complexes on surfaces and in solutions. *Inorg Chem* 29:1536–1543.
- Olivier D, Vedrine JC, Pezerat H. 1975. Application de la résonance paramagnétique électronique à la localisation du Fe^{3+} dans les smectites. *Bull Groupe Franç Argiles* 27:153–165.
- Schweiger A. 1991. Pulsed electron spin resonance spectroscopy: Basic principles, techniques, and examples of applications. *Angew Chem Int Engl* 30:265–292.
- Suquet H, Mallard C, Quarton M, Dubernat J, Perzerat H. 1984. Etude du biopyribole formé par chauffage des vermiculites magnésiennes. *Clay Miner* 19:217–227.
- Suquet H, Chevalier S, Marcilly C, Barthomeuf D. 1991. Preparation of porous materials by chemical activation of the Llano vermiculite. *Clay Miner* 26:49–60.
- Veblen DR. 1991. Polysomatism and polysomatic series: A review and applications. *Am Mineral* 76:801–826.
- Veblen DR, Buseck P. 1980. Microstructures and reaction mechanisms in biopyriboles. *Am Mineral* 65:599–623.
- Wildemann TR. 1970. The distribution of Mn^{2+} in some carbonates by electron paramagnetic resonance. *Chem Geol* 5:167–177.

(Received 10 March 1995; accepted 22 September 1995; Ms. 2634)